NONISOTHERMAL REACTIVE TRANSPORT MODELS OF CONCRETE/BENTONITE COLUMN TESTS

J. Samper[1]*, A. Mon[1], L. Montenegro[1], A. Naves[1], J. Fernández[1], J. Cuevas[2], R. Fernández[2], M. J. Turrero[3] y E. Torres[3]

[1] Centro de Investigaciones Científicas Avanzadas, Escuela de Caminos, Canales y Puertos, Universidade da Coruña, Campus de Elviña s/n 15071 A Coruña. e-mail: j.samper@udc.es.
[2] Facultad de Ciencias, Universidad Autónoma de Madrid. Ciudad Universitaria de Cantoblanco, Calle Francisco Tomás y Valiente, 7, 28049 Madrid. e-mail: jaime.cuevas@uam.es.
[3] Centro de Investigaciones Energéticas, Medio Ambientales y Tecnológicas. Av. Complutense, 40, 28040 Madrid. e-mail: mj.turrero@ciemat.es.

RESUMEN. El almacenamiento geológico profundo de residuos radiactivos contempla el uso de barreras de bentonita compactada y revestimientos de hormigón. Las condiciones alcalinas causadas por la degradación del hormigón pueden afectar a la integridad de la barrera bentonítica. En este trabajo se presentan modelos acoplados térmicos, hidrodinámicos, geoquímicos y mecánicos de una serie de ensayos de hidratación y calentamiento realizados en el CIEMAT en columnas de bentonita y hormigón (Turrero et al. 2011; Torres et al. 2013) para estudiar las interacciones geoquímicas en la interfaz hormigón-bentonita en las condiciones no isotermas y no saturadas previstas después de la clausura de un almacenamiento de residuos radiactivos de alta actividad. Los ensayos se realizaron con duraciones comprendidas entre 6 y 104 meses. Los resultados de los modelos reproducen las tendencias generales de los datos medidos de contenido de humedad, porosidad y temperatura y las observaciones experimentales cualitativas de las fases minerales.

ABSTRACT. Radioactive waste disposal in deep geological repositories in clay formations envisage com-pacted bentonite engineered barriers and concrete liners. The alkaline conditions caused by the degradation of concrete could affect the performance of the bentonite barrier. Here we present coupled thermal, hydrodynamic, chemical and mechanical models of several heating and hydration concrete/bentonite column tests, which were performed by CIEMAT (Turrero et al. 2011; Torres et al. 2013) to study the geochemical interactions occurring at the concrete-bentonite interface for the non-isothermal unsaturated conditions prevailing after the closure of a high-level radioactive waste repository. The tests lasted from 6 to 104 months. Model results reproduce the general trends of the measured water content, porosity, temperature and the observed qualitative patterns of mineral phases.

1.- Introduction

Compacted bentonite is a backfill and sealing material for high-level radioactive waste (HLW) disposal in deep geological repositories. A concrete liner will be the support of the galleries in the Spanish Reference Concept for disposal in a clay host rock (ENRESA, 2004). Concrete is a source of alkaline solutions, which may reduce the porosity at its interfaces with other materials due to the precipitation of mineral phases.

CIEMAT performed several heating and hydration concrete/bentonite column tests to study the geochemical interactions occurring at the concrete-bentonite interface for the non-isothermal unsaturated conditions prevailing after the closure of a high-level radioactive waste repository (Turrero et al. 2011; Torres et al. 2013). The tests are denoted as HB ("Hormigón-Bentonita") tests. The HB column tests were dismantled after 6, 12, 18, 54, 80 and 104 months for the HB1 to the HB6 tests. Thyey provide data on the concrete and bentonite interactions after contact times ranging from 6 to 104 months.

The geochemical evolution of the bentonite barrier during the initial stages of the hydration and heating of the repository depends on the thermal, hydrodynamic and mechanical processes (Samper et al. 2008a; Zheng and Samper, 2008; Zheng et al, 2008a, 2008b, 2010, 2011). Thus, coupled thermo-hydro-chemical-mechanical, (THCM) numerical models are required. Here we present the coupled THCM models of the entire set of the HB column tests. In addition, we report a sensitivity analysis of the model results for the HB4 column test.

2.- HB column tests

The HB column tests were performed on cells containing a 7.15 cm thick bentonite sample in contact with a 3 cm thick concrete sample. The concrete was made of sulphate-resistant ordinary Portland cement, OPC, (CEM I-SR) following the mix by CSIC-IETcc: 400 kg of CEM I-SR cement, 911 kg of sand (0-5 mm), and 946 kg of aggregates (6-16 mm) with a w/c ratio of 0.45. The bentonite was FEBEX bentonite from the Cortijo de Archidona. The bentonite blocks were compacted with a gravimetric water content of 14% and a dry density of 1.65 Mg/m^3. The cells were hydrated with the synthetic Spanish Reference Clay porewater (RAF water, Turrero et al. 2011). The cells were hydrated at a constant pressure (Figure 1).

The initial porosity of the bentonite is 0.4, which corresponds to a water saturation of 57% and a suction of $1.27 \cdot 10^8$ Pa. The concrete has a porosity of 0.125 and a gravimetric water content of 2.2%. The initial temperature is 22ºC along the cell. The temperature of the hydration water is 25ºC. The prescribed temperature at the bottom of the column, where the heater is located, is 90 °C. This temperature is lower than the heater temperature due to lateral heat losses. Relative humidity and

temperature in the bentonite were monitored during the tests at 50 and 95 mm from the hydration boundary. Water content and dry density were measured along the cells at the end of the tests. The relative humidity data measured in the sensor located near the heater are judged to be unreliable because these data are affected by vapor leakage through the sensors.

HB1, HB2 and HB3 column tests were dismantled after 6, 12 and 18 months, respectively within the framework of the NFPRO EU Project (Near Field Processes Project). HB4 and HB5 tests were dismantled after 54 and 80 months within the context of the PEBS EU Project (Long-term Performance of Engineered Barrier Systems). The HB6 column test was dismantled after 104 months within the framework of the CEBAMA EU Project (Cement-based materials, properties, evolution, barrier functions)). The laboratory observations of mineral patterns from HB5 and HB6 tests are not yet available for modelling.

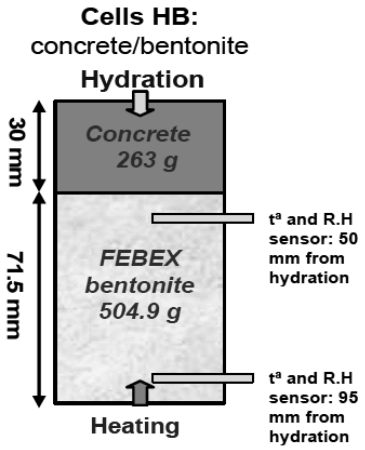

Fig. 1. Setup of the concrete-bentonite HB column tests (Turrero et al. 2011).

2.- Model description

The models assume that the thermal, hydrodynamic and solute transport processes occur mostly in the longitudinal direction (along the direction of the axis of the cells). The HB column tests were modelled with a 1D grid (see Figure 2). The model includes two materials, the concrete ($0 < x < 3$ cm), and the bentonite (3 cm $< x < 10.15$ cm). The cells constrained partly the deformation of the bentonite blocks. The model accounts for bentonite swelling and allows for the displacement of the bentonite column to simulate the measured deformation. No concrete vertical displacement was allowed in the model because the concrete is not expected to deform.

Bentonite and concrete parameters were taken from previous models of the HB4 test (Samper et al. 2013, 2017, 2018b). Similar to previous THCM models of the FEBEX bentonite (Zheng et al. 2010), the initial total stress was assumed uniform and equal to 250 kPa. There were experimental problems to maintain a constant water injection pressure during some of the tests. Given the lack of reliable water injection pressure data, the liquid injection pressure was estimated from measured cumulative inflow data. Its value is equal to 100 kPa (Samper et al. 2018a).

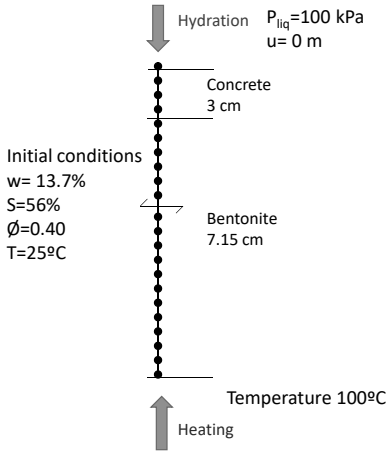

Fig. 2. Finite element mesh and boundary conditions for the numerical model of the HB column tests.

The geochemical model accounts for the following reactions: 1) Aqueous complexation; 2) Acid/base; 3) Cation exchange of Ca^{2+}, Mg^{2+}, Na^{+} and K^{+}; 4) Surface complexation of H^{+} in three types of sorption sites (SS-OH, SW1-OH and SW2-OH) and; 5) mineral dissolution/precipitation. The chemical system is defined in terms of the concentrations of the following primary species: H_2O, H^{+}, Ca^{2+}, Mg^{2+}, Na^{+}, K^{+}, Cl^{-}, SO_4^{2-}, HCO_3^{-}, SiO_2(aq) and Al^{3+}. The model takes into account 42 aqueous species and 12 minerals. Cation exchange reactions were modelled with the Gaines-Thomas convention. The triple sorption site model of Bradbury and Bayens (1997; 2003) is used for the surface complexation. Chemical reactions and their equilibrium constants, K, at 25ºC for the aqueous complexes, mineral phases, selectivity coefficients and protolysis constants are listed in Table 1. It should be pointed out that the values of log K have uncertainties. Model results are strongly dependent on the values of the log K. Therefore, the uncertainties in log K values lead to model uncertainties.

The initial composition of the OPC concrete porewater was derived from speciation runs performed with the code EQ3/6 (Wolery 1992) by assuming that the concentration of dissolved Ca^{2+} is controlled by local chemical equilibrium with respect to portlandite, HCO_3^{-} concentration is at equilibrium with respect to calcite, Mg^{2+} concentration is derived from the equilibration with brucite, Al^{3+} is at equilibrium with ettringite and SiO_2(aq) is controlled by equilibrium with respect to C1.8SH. The initial mineral volume fractions in the concrete are: 7.4% for portlandite, 2.2% for ettringite, 14.6% for C1.8SH, 1% for brucite, 0.1% for calcite and 62.2% for quartz. Quartz is assumed to be nonreactive. The initial pore water composition of the FEBEX bentonite was taken from Fernández et al. (2004). The initial mineral volume fractions in the bentonite are: 0.36% for calcite, 0.0829%

for gypsum, 1.18% for cristobalite; and 57% for the nonreactive smectite. The smectite was assumed to be unreactive. The model allows for the precipitation of the following secondary minerals: sepiolite, C0.8SH, anorthite and anhydrite. The dissolution/precipitation of portlandite, ettringite, C1.8SH, C0.8SH, quartz and cristobalite was simulated with the kinetic rate laws of Fernández et al. (2009). Cation exchange and proton surface complexation reactions were assumed to take place only in the bentonite (Huertas et al. 2001).

The models were solved with INVERSE-FADES-CORE V2, a code developed at the University of A Coruña (UDC) (Zheng et al. 2011; Mon, 2017). This is part of a series of reactive transport codes developed at UDC (Samper et al. 2008b; Soler et al. 2008; Yang et al. 2008).

3.- Model results

3.1.- THM results

The computed water content and porosity reproduce the general trends of the measured data at the end of the HB1 to HB 4 tests (see Figures 3 and 4). The concrete is fully saturated after 7 days and then, the bentonite hydrates at a very low rate through the concrete. Water content increases near the concrete and decreases near the heater due to the evaporation. The volumetric water content increases in the bentonite near the concrete interface and reaches a maximum value of 0.5 at 7 days. The porosity increases in the bentonite near the concrete interface due to bentonite swelling and decreases slightly near the heater. The hydrodynamic results of the HB1 to HB6 column tests are similar because the water intake is fast in the first months and slows down after 10 months.

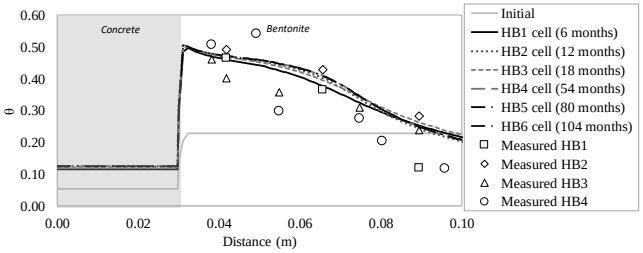

Fig. 3. Computed volumetric water content (lines) and measured data (symbols) for the HB1, HB2, HB3, HB4, HB5 and HB6 column tests.

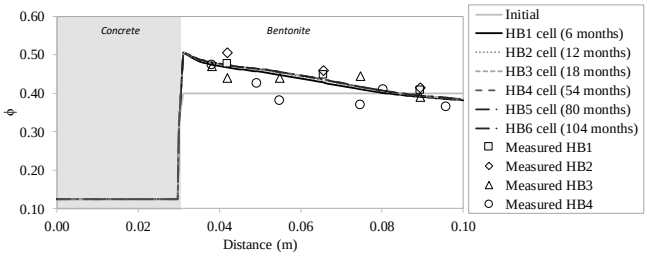

Fig. 4. Computed porosity (lines) and measured data (symbols) for the HB1, HB2, HB3, HB4, HB5 and HB6 column tests.

Table 1. Chemical reactions and equilibrium constants for aqueous complexes and minerals (Wolery, 1992), protolysis constants for surface complexation reactions (Bradbury and Baeyens, 1997) and selectivity coefficients for cation exchange reactions (Huertas et al. 2001; ENRESA, 2006) at 25ºC.

Aqueous complexes	**Log K**
$CaCO_3(aq) + H^+ \Leftrightarrow Ca^{2+} + HCO_3^-$	7.0017
$CaHCO_3^+ \Leftrightarrow Ca^{2+} + HCO_3^-$	-1.0467
$CaSO_4(aq) \Leftrightarrow Ca^{2+} + SO_4^{2-}$	-2.1111
$CaCl^+ \Leftrightarrow Ca^{2+} + Cl^-$	0.6956
$CaOH^+ + H^+ \Leftrightarrow Ca^{2+} + H_2O$	12.850
$CO_2(aq) + H_2O \Leftrightarrow H^+ + HCO_3^-$	-6.3447
$CO_3^{2-} + H^+ \Leftrightarrow HCO_3^-$	10.3288
$KSO_4^- \Leftrightarrow K^+ + SO_4^{2-}$	-0.8796
$MgCO_3(aq) \Leftrightarrow Mg^{2+} + CO_3^{2-}$	-2.9789
$MgHCO_3^+ \Leftrightarrow Mg^{2+} + HCO_3^-$	-1.0357
$MgSO_4(aq) \Leftrightarrow Mg^{2+} + SO_4^{2-}$	-2.4117
$MgCl^+ \Leftrightarrow Mg^{2+} + Cl^-$	0.1349
$NaHCO_3(aq) \Leftrightarrow Na^+ + HCO_3^-$	-0.1541
$NaSO_4^- \Leftrightarrow Na^+ + SO_4^{2-}$	-0.8200
$NaCO_3^- + H^+ \Leftrightarrow Na^+ + HCO_3^-$	9.8367
$NaCl(aq) \Leftrightarrow Na^+ + Cl^-$	0.7770
$NaOH(aq) + H^+ \Leftrightarrow Na^+ + H_2O$	14.1800
$H_3SiO_4^- + H^+ \Leftrightarrow SiO_2(aq) + 2H_2O$	9.8120
$OH^- + H^+ \Leftrightarrow H_2O$	13.9951
$CaCl_2(aq) \Leftrightarrow Ca^{2+} + 2Cl^-$	0.6436
$Ca(H_3SiO_4)_2(aq) + 2H^+ \Leftrightarrow Ca^{2+} + 2SiO_2(aq) + 4H_2O$	15.0532
$CaH_2SiO_4(aq) + 2H^+ \Leftrightarrow Ca^{2+} + SiO_2(aq) + 2H_2O$	18.5616
$CaH_3SiO_4^+ + H^+ \Leftrightarrow Ca^{2+} + SiO_2(aq) + 2H_2O$	8.7916
$MgOH^+ + H^+ \Leftrightarrow Mg^{2+} + H_2O$	11.607
$Mg_4(OH)_4^{4+} + 4H^+ \Leftrightarrow 4Mg^{2+} + 4H_2O$	39.750
$MgH_2SiO_4(aq) + 2H^+ \Leftrightarrow Mg^{2+} + SiO_2(aq) + 2H_2O$	17.4816
$MgH_3SiO_4^+ + H^+ \Leftrightarrow Mg^{2+} + SiO_2(aq) + 2H_2O$	8.5416
$NaH_3SiO_4(aq) + H^+ \Leftrightarrow 2H_2O + Na^+ + SiO_2(aq)$	8.6616
$NaHSiO_3(aq) + H^+ \Leftrightarrow H_2O + Na^+ + SiO_2(aq)$	8.3040
$KOH(aq) + H^+ \Leftrightarrow K^+ + H_2O$	14.4600
$KCl(aq) \Leftrightarrow K^+ + Cl^-$	1.4946
$KHSO_4(aq) \Leftrightarrow H^+ + K^+ + SO_4^{2-}$	-0.8136
$H_2SiO_4^{2-} + 2H^+ \Leftrightarrow 2H_2O + SiO_2(aq)$	22.9116
$H_4(H_2SiO_4)_4^{4-} + 4H^+ \Leftrightarrow 8H_2O + 4SiO_2(aq)$	35.7464
$HSiO_3^- + H^+ \Leftrightarrow H_2O + SiO_2(aq)$	9.9525
$H_6(H_2SiO_4)_4^{2-} + 2H^+ \Leftrightarrow 8H_2O + 4SiO_2(aq)$	13.4464
$HCl(aq) \Leftrightarrow H^+ + Cl^-$	0.6700
$HSO_4^- \Leftrightarrow H^+ + SO_4^{2-}$	1.9791
$Al(OH)_4^- + 4H^+ \Leftrightarrow Al^{3+} + 4H_2O$	22.1477
$Al(OH)_3(aq) + 3H^+ \Leftrightarrow Al^{3+} + 3H_2O$	16.1577
$Al(OH)_2^+ + 2H^+ \Leftrightarrow Al^{3+} + 2H_2O$	10.0991
$AlOH^{2+} + H^+ \Leftrightarrow Al^{3+} + H_2O$	5.0114
Minerals	**Log K**
$Calcite + H^+ \Leftrightarrow Ca^{2+} + HCO_3^-$	1.8487
$Anhydrite \Leftrightarrow Ca^{2+} + SO_4^{2-}$	-4.3064
$Gypsum \Leftrightarrow Ca^{2+} + SO_4^{2-} + 2H_2O$	-4.4823
$Cristobalite \Leftrightarrow SiO_2(aq)$	-3.4488
$Quartz \Leftrightarrow SiO_2(aq)$	-3.9993
$Portlandite + 2H^+ \Leftrightarrow Ca^{2+} + 2H_2O$	22.5552
$Brucite + 2H^+ \Leftrightarrow Mg^{2+} + 2H_2O$	16.2980
$Sepiolite + 8H^+ \Leftrightarrow 4Mg^{2+} + 6SiO_2(aq) + 11H_2O$	30.4439
$C1.8SH + 3.6H^+ \Leftrightarrow 1.8Ca^{2+} + SiO_2(aq) + 2.8H_2O$	32.4814
$C0.8SH + 1.6H^+ \Leftrightarrow 0.8Ca^{2+} + SiO_2(aq) + 1.8H_2O$	10.8614
$Ettringite + 12H^+ \Leftrightarrow 2Al^{3+} + 3SO_4^{2-} + 6Ca^{2+} + 38H_2O$	60.8127
$Anorthite + 8H^+ \Leftrightarrow Ca^{2+} + 2Al^{3+} + 2SiO_2(aq) + 4H_2O$	24.8686
Surface complexation reactions	**Log K**
$\equiv S^SOH_2^+ \Leftrightarrow \equiv S^SOH + H^+$	-4.5
$\equiv S^SO^- + H^+ \Leftrightarrow S^SOH$	7.9
$\equiv S^{W1}OH_2^+ \Leftrightarrow \equiv S^{W1}OH + H^+$	-4.5
$\equiv S^{W1}O^- + H^+ \Leftrightarrow \equiv S^{W1}OH$	7.9
$\equiv S^{W2}OH_2^+ \Leftrightarrow \equiv S^{W2}OH + H^+$	-6.0
$\equiv S^{W2}O^- + H^+ \Leftrightarrow \equiv S^{W2}OH$	-10.5
Cation exchange reactions	**$K_{Na\text{-}cation}$**

$Na^+ + X\text{-}K \Leftrightarrow K^+ + X\text{-}Na$	0.1456
$Na^+ + 0.5\ X_2\text{-}Ca \Leftrightarrow 0.5\ Ca^{2+} + X\text{-}Na$	0.3265
$Na^+ + 0.5\ X_2\text{-}Mg \Leftrightarrow 0.5\ Mg^{2+} + X\text{-}Na$	0.3766

3.1.- Chemical results

Calcite is initially present in the concrete and in the bentonite. Calcite precipitates slightly in the concrete near the hydration zone because the concentration of dissolved Ca^{2+} in the hydration water is larger than that of the initial concrete porewater. Calcite precipitates at both sides of the concrete/bentonite interface, being larger in the concrete near such interface. The precipitation front of calcite penetrates 0.95 cm into the bentonite and 0.4 cm into the concrete after 104 months. The precipitation and dissolution front of calcite in the bentonite advances with time. Portlandite dissolves throughout the concrete domain, and especially near the concrete/bentonite interface. C1.8SH dissolves in the concrete, except near the hydration boundary where it precipitates because the dissolved concentrations of SiO_2(aq) and Ca^{2+} in the boundary water are larger than those of the concrete porewater (Samper et al. 2018b).

Brucite precipitates near the hydration boundary because the concentration of dissolved Mg^{2+} in the hydration water is larger than that of the initial concrete porewater. Brucite precipitates also in the concrete and the bentonite near the concrete/bentonite interface. The peaks of precipitation are located in the concrete. The front of brucite precipitation spreads 0.21 cm into the concrete and 0.8 cm into the bentonite after 104 months. Sepiolite precipitates in narrow bands at both sides of the concrete/bentonite interface in the HB1, HB2, HB3 and HB4 column tests. Later, sepiolite dissolves in the concrete and extends 0.48 and 0.8 cm in the bentonite for the HB5 and HB6 column tests, respectively.

Gypsum dissolves initially because the initial bentonite water is not in equilibrium with gypsum. It precipitates in the bentonite near the concrete/bentonite interface in HB1 column test and near the heater in the HB4 column test. A precipitation front of anhydrite moving in the bentonite to the heater side is calculated in the models of the HB1, HB2 and HB3 column tests. Gypsum and anhydrite are not present at the end of the HB5 and HB6 tests. Model results show very small values of precipitation or dissolution of cristobalite, quartz, CSH0.8 and ettringite.

Figure 5 to Figure 10 show the computed pH and the mineral volume fractions for the HB1 to HB6 tests. The penetration of the pH front into the bentonite increases with time. The high pH plume (pH > 8.5) penetrates 0.23, 0.32, 1.04, 5.8 and 6.7 cm into the bentonite at the end of the HB1, HB2, HB3, HB4, HB5 and HB6 tests, respectively. The diffusion of the alkaline plume is retarded by the precipitation of brucite in the concrete and calcite and sepiolite in the bentonite. The final pH in the concrete near the hydration boundary (x=0) is around 12. The pH in the bentonite near the concrete/bentonite interface (x=0.03 m) in the HB1, HB2 and HB3 column tests is equal to 9.5 and around 11 for the HB4, HB5 and HB6 column tests.

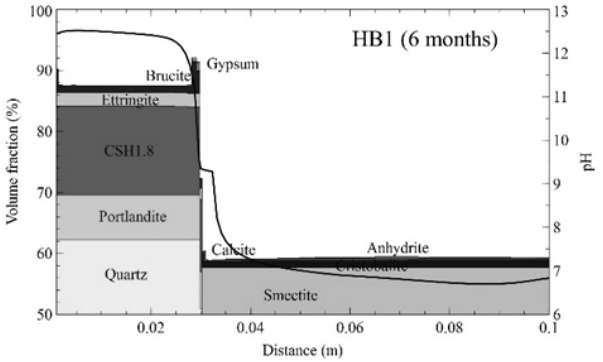

Fig. 5. Computed pH and mineral volume fractions for the HB1 test.

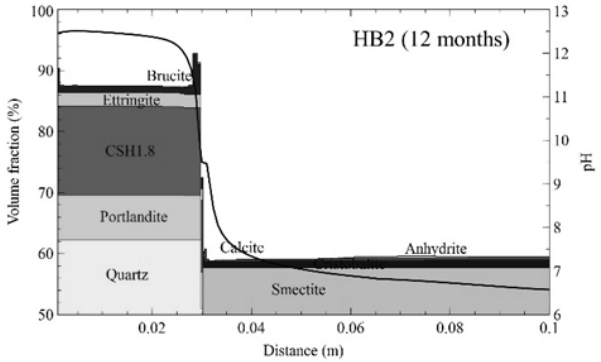

Fig. 6. Computed pH and mineral volume fractions for the HB2 column test.

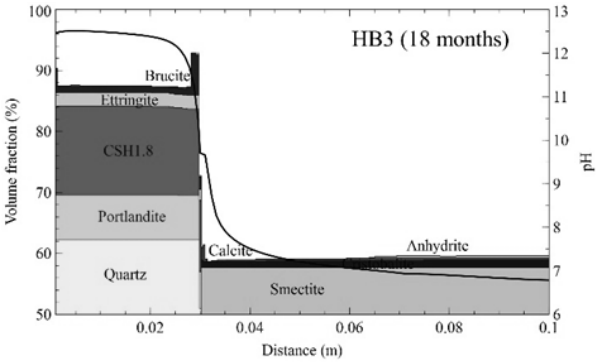

Fig. 7. Computed pH and mineral volume fractions for the HB3 test.

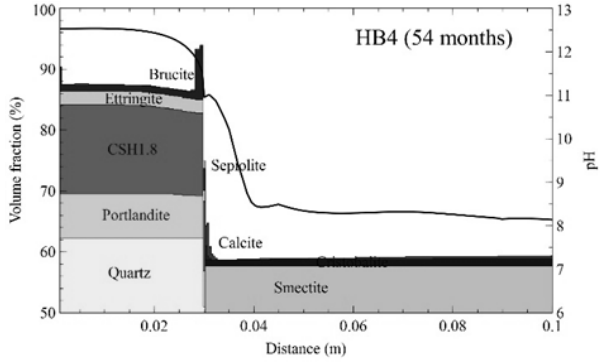

Fig. 8. Computed pH and mineral volume fractions for the HB4 test.

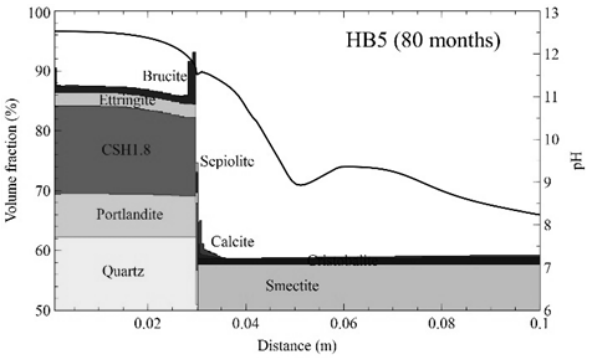

Fig. 9. Computed pH and mineral volume fractions for the HB5 test.

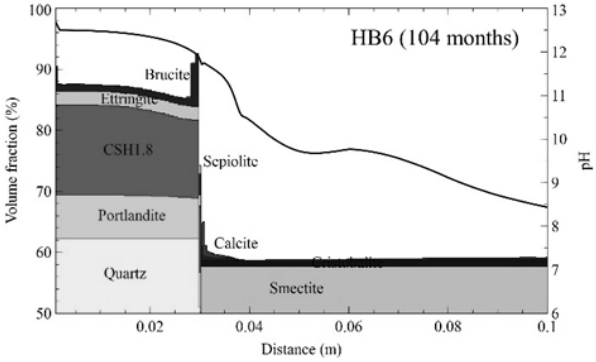

Fig. 10. Computed pH and mineral volume fractions for the HB6 test.

A qualitative comparison of the computed values and the experimental mineral observations reveals that the numerical model captures the main trends of the experimental mineralogical observations (Table 2). However, there are some discrepancies for ettringite and C-S-H precipitation. The numerical model predicts ettringite dissolution and a very small precipitation of C-S-H. Model discrepancies could be caused by uncertainties in: 1) The selection of the appropriate C-S-H, M-S-H and C-A-S-H phases; 2) The kinetic parameters (rate laws and specific surfaces); and 3) The selection of the appropriate secondary clay minerals.

We recall that the numerical model accounts for the changes in porosity caused by mechanical processes, but the changes in porosity due to mineral dissolution/precipitation are not considered. Porosity decreases in the concrete/bentonite interface and at the hydration boundary mainly due to brucite and calcite precipitation. The porosity at end of the HB6 column test decreases 24% near the hydration zone due to brucite precipitation, increases about 10% in the interval 0.02 m < x < 0.029 m due to the simultaneous dissolution of C1.8SH, portlandite and ettringite dissolution and reduces about 40% in the concrete near the concrete/bentonite interface (in a 0.04 cm zone) due to brucite and calcite precipitation.

4.- Sensitivity analyses

Numerical models have uncertainties due to uncertainties in the values of the model parameters, the boundary conditions, the geochemical assumptions of the model and the discretization parameters. These uncertainties are quantified by performing model sensitivity runs in which model parameters or assumptions are changed, usually one at a time. This section presents the results of the following sensitivity runs performed with the model of the HB4 column testd: 1) isothermal versus non-isothermal conditions; 2) the changes in the specific surfaces of kinetically-controlled minerals; and 3) the grid size of the finite element mesh.

4.1.- Sensitivity to the thermal field

The base run of the HB4 column test is non-isothermal. A sensitivity run was performed at a constant and uniform temperature of 25ºC. Figure 11 and Figure 12 show the computed cumulative precipitation of calcite and brucite for the base and sensitivity runs. The model results for constant temperature show significant differences in the precipitation of calcite and brucite. The peaks of brucite and calcite precipitation for constant temperature are smaller than those of the base run. Moreover, the thickness of the bentonite zone where calcite and brucite precipitate in the constant temperature run is larger than that of the base run. Brucite precipitates in the concrete and in the bentonite in the base run, while it precipitates only in the bentonite in the constant temperature run.

The reduction in porosity in the concrete near the bentonite interface and in the bentonite in the constant temperature run is smaller than that of the base run (Figure 13). All these differences in the computed mineral precipitation and porosity reduction between the isothermal and non-isothermal runs are mainly related to changes in the equilibrium constants, which depend on temperature, and water evaporation near the heater, which occurs only in the non-isothermal model run.

4.2.- Sensitivity to mineral kinetics

Sensitivity runs were performed to investigate the response of the model results to changes in the specific surfaces of kinetically-controlled portlandite and ettringite. Model results are sensitive to an increase of the specific surface of portlandite by a factor of 2 and an increase of the specific surface of ettringite by a factor of 10 (Fig 14). The increase in the specific surface of portlandite leads to larger portlandite dissolution rates, larger calcite precipitation and larger pH in the bentonite. The increase in the specific surface of ettringite leads to more precipitation of ettringite in the upstream part of the concrete, more ettringite dissolution in the concrete near the bentonite interface and larger pH in the bentonite. The model lacks sensitivity to the kinetic Mg-saponite precipitation (Fig 14), which was simulated with the kinetic law reported by Mon et al. (2017).

4.3.- Sensitivity to grid size

Grid size in the reference model is uniform and equal to 0.9 mm. Several sensitivity runs were performed in which the grid was refined in a 3 cm wide band around the concrete/bentonite interface. Grid sizes of 0.45 mm, 0.18 mm and 0.1 mm were considered in three sensitivity runs while the size of the rest of the elements was equal to 0.45 mm.

The numerical solution improves when the grid size decreases because the discretization errors decrease when the grid size decreases. Model results for the run with the smallest grid size are considered the most realistic.

Mineral precipitation increases at both sides of the concrete/bentonite interface when the grid size is reduced (Figure 15). The calculated porosity in the concrete near the bentonite interface decreases drastically, reaching pore clogging for grid sizes smaller than 0.18 mm.

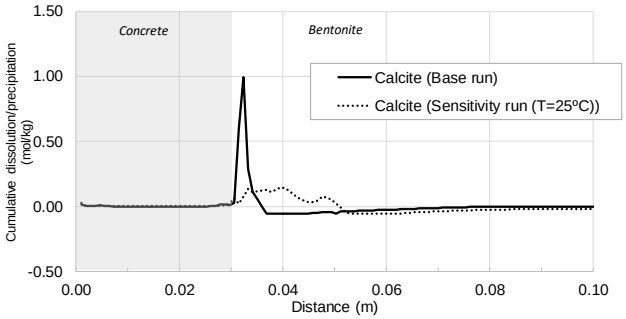

Fig. 11. Computed calcite precipitation/dissolution for the base and the sensitivity run with a uniform temperature (25ºC) for the model of the HB4 column test.

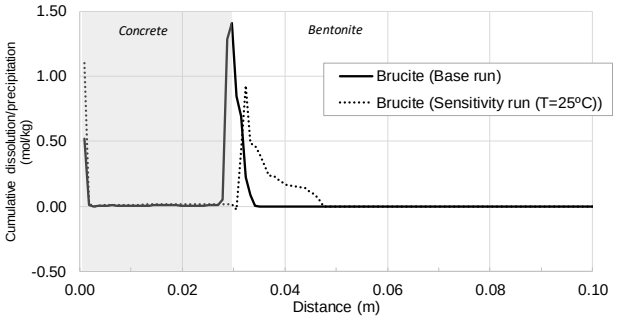

Fig. 12. Computed brucite precipitation/dissolution for the base and the sensitivity run with a uniform temperature (25ºC) for the model of the HB4 column test.

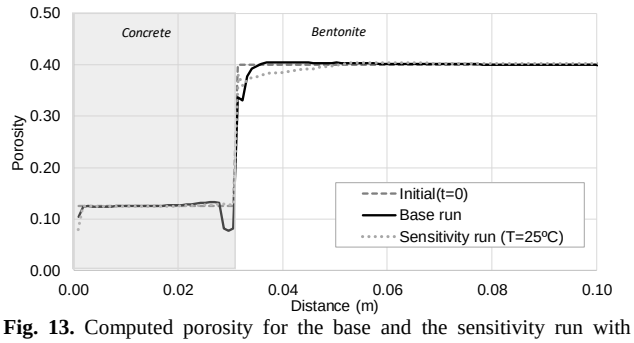

Fig. 13. Computed porosity for the base and the sensitivity run with a uniform of 25ºC temperature for the model of the HB4 column test.

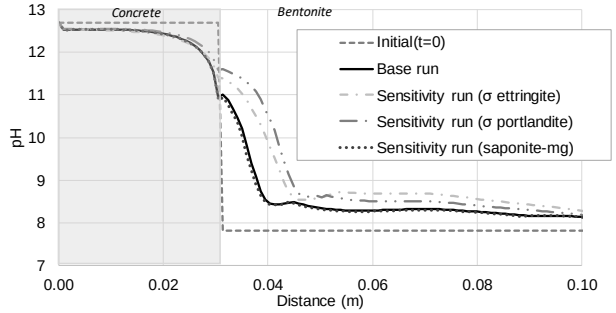

Fig. 14. Model of the HB4 column test: Sensitivity of the computed pH to changes in the mineral kinetic parameters.

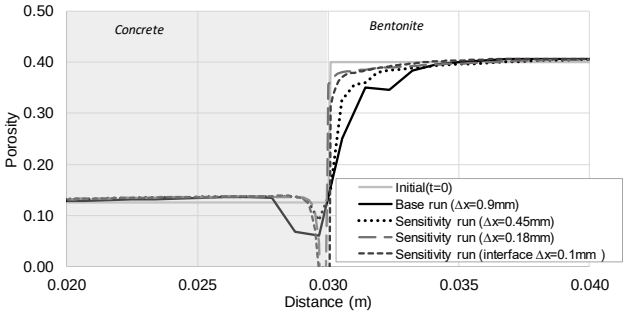

Fig. 15. Model of the HB4 column test: Sensitivity of the computed porosity to changes in the grid size.

5.- Conclusions and future work

Coupled THCM models of the HB1, HB2, HB3, HB4, HB5 and HB6 tests have been presented. Model results reproduce the general trends of the measured water content, porosity, and temperature (not shown here) and the observed patterns of mineral phases for the HB1 to HB4 tests. The predictions of the HB5 and HB6 tests show similar trends to those of the rest of the tests. These predictions will be compared to measured data when they become available.

The results of the isothermal sensitivity run attest the conclusions of Lalan et al. (2016) who concluded that the temperature plays an important role in the degradation of C-S-H and the precipitation of mineral phases. The thickness of the bentonite zone where calcite and brucite precipitate in the constant temperature run is larger than that of the base run. While brucite precipitates in the concrete and in the bentonite in the base run, it precipitates only in the bentonite in the constant temperature run. The reduction in porosity in the concrete near the bentonite interface and in the bentonite in the constant temperature run is smaller than that of the base run. The intricate interplays of thermal and chemical processes in this complex chemical system prevent a simple explanation for the results of the sensitivity run to temperature.

Model results are sensitive to the increase of the specific surfaces of portlandite and ettringite. On the other hand, model results are not sensitive to kinetic

Mg-saponite precipitation. Mineral precipitation increases at both sides of the concrete/bentonite interface when the grid size is reduced. The calculated porosity in the concrete near the bentonite interface decreases drastically, reaching pore clogging for grid sizes smaller than 0.18 mm.

The models presented here account for the changes in porosity caused by solid deformation and swelling, but disregard the changes in porosity due to mineral dissolution/precipitation because the mechanical changes in porosity for bentonite are generally larger than the chemical changes in porosity (Mon, 2017; Samper et al. 2018b). The THCM models of the HB column tests could be improved by: 1) considering additional C-S-H and M-S-H phases; 2) adjusting the kinetic parameters and 3) accounting for the feedback effect of the changes in porosity caused by mineral dissolution/precipitation.

Acknowledgements. "The research leading to these results has received funding from the European Union's European Atomic Energy Community's (Euratom) Horizon 2020 Programme (NFRP-2014/2015) under grant agreement, 662147 – Cebama". This work was partly funded by the Spanish Ministry of Economy and Competitiveness (Project CGL2016-78281), FEDER funds and the Galician Regional Government (Project ED431C 2017/67 from "Consolidación e estruturación de unidades de investigación competitivas", Grupos de referencia competitiva).

7.- Bibliografía

Bradbury, M.H. and B. Baeyens, 1997. A mechanistic description of Ni and Zn sorption on Na-montmorillonite. Part II: modelling. *J. Contam. Hydrol.* 27, 223–248.

Bradbury, M.H. and B. Baeyens, 2003. Pore water chemistry in compacted resaturated MX-80 bentonite. *J. Contam. Hydrol*. 61, 329–338.

ENRESA, 2004. Evaluación del comportamiento y de la seguridad de un almacén geológico profundo de residuos radiactivos en arcilla. PT 49-1PP-M-A1-01. [in Spanish].

ENRESA, 2006. FEBEX : Final THG Modelling Report. ENRESA Tech. Publ. PT 05-03/2006, 155 pp.

Fernández A.M., B. Baeyens, M. Bradbury and P. Rivas, 2004. Analysis of pore water chemical composition of a Spanish compacted bentonite used in an engineered barrier. *Phys. Chem. Earth* 29, 105-118.

Fernández R., J. Cuevas and U. K. Mäder, 2009. Modelling concrete interaction with a bentonite barrier. *Eur. J. Mineral.* 21, 177-191.

Huertas, F.J., P. Carretero, J. Delgado, J. Linares, & J. Samper, 2001, An experimental study on the ion exchange behavior of the FEBEX bentonite, Journal of Colloid and Interface Science, Vol 239, 409-416.

Lalan P., A. Dauzères, L. DeWindt, D. Bartier, J. Sammaljärvi, J.D. Barnichon, I. Techer and V. Detilleux 2016. Impact of a 70 °C temperature on an ordinary Portland cement paste/claystone interface: An in situ experiment. *Cement Concr. Res.* 83, 164-178.

Mon A., 2017. Coupled thermo-hydro-chemical-mechanical models for the bentonite barrier in a radioactive waste repository. Ph. D. Dissertation. Universidad de A Coruña, Spain.

Mon A., J. Samper, L. Montenegro, A. Naves and J. Fernández, 2017. Long-term non-isothermal reactive transport model of compacted bentonite, concrete and corrosion products in a HLW repository in clay. *J. Contam. Hydrol.*, 197, 1-16.

Samper, J., L. Zheng, L. Montenegro, A.M. Fernández and P. Rivas, 2008a. Testing coupled thermo-hydro-chemical models of compacted bentonite after dismantling the FEBEX in situ test. *Appl. Geochem.* (23/5), 1186–1201.

Samper, J., Lu, C., Montenegro, L., 2008b. Reactive transport model of interactions of corrosion products and bentonite. Phys. Chem. Earth 33 (Suppl. 1), S306–S316.

Samper J., A. Mon, L. Montenegro, B. Pisani and A. Naves, 2013. Report on testing multiple-continua THCM models with laboratory and large-scale tests. Deliverable 3.4-1 of the PEBS Project.

Samper, J., A. Mon, L. Montenegro, A. Naves, J Fernández, J. Cuevas, R. Fernández, M.J. Turrero and E. Torres, 2017. Coupled THCm numerical models of heating and hydration tests to study the interactions of compacted FEBEX bentonite with OPC concrete. Proceedings of the First Annual Workshop of the HORIZON 2020 CEBAMA Project, M. Altmaier, V. Montoya, L. Duro Ed.

Samper, J., A. Mon, L. Montenegro, A. Naves, J Fernández, J. Cuevas, R. Fernández, M.J. Turrero and E. Torres, 2018a. Coupled THCM models of heating-hydration tests containing OPC concrete and compacted FEBEX bentonite. Proceedings of the Third Annual Workshop of the HORIZON 2020 CEBAMA Project, M. Altmaier, V. Montoya, L. Duro Ed.

Samper, J, A. Mon, L. Montenegro, J. Cuevas, M. J. Turrero, A. Naves, R. Fernández and E. Torres, 2018b. Coupled THCM model of a heating and hydration concrete-bentonite column test. *Applied Geochemistry* 94, 67-81.

Soler J.M, J. Samper, A. Yllera, A. Hernández, A. Quejido, M. Fernández, C. Yang, A. Naves, P. Hernán, and P. Wersin, 2008, The DI-B in-situ diffusion experiment at mont terri: results and modelling, Physics and Chemistry of the Earth, Vol. 33. Supplement 1, 2008, S196-S207.

Torres E., M.J. Turrero, A. Escribano and P.L. Martín, 2013. Geochemical interactions at the concrete-bentonite interface of column experiments. Deliverable 2.3-6-1 of PEBS Project.

Turrero M. J., M. V. Villar, E. Torres, A. Escribano, J. Cuevas, R. Fernández, A. I. Ruiz, R. Vigil de la Villa and I. del Soto, 2011. Laboratory tests at the interfaces. Final results of the dismantling of the tests FB3 and HB4. Deliverable 2.3-3-1 of PEBS Project.

Wolery T.J., 1992. EQ3/3. A software package for geochemical modeling of aqueous system: package overview and installation guide version 7.0. UCRL-MA-110662-PT-I, Lawrence Livermore National Laboratory, Livermore, California.

Yang, C, J. Samper and J. Molinero, 2008, Inverse microbial and geochemical reactive transport models in porous media, Physics and Chemistry of the Earth, Vol. 33 Issues 12-13: 1026-1034.

Zheng, L. and J. Samper, 2008. A coupled THMC model of FEBEX mock-up test. *Phys. Chem. Earth* 33, S486–S498.

Zheng, L., J. Samper, and L. Montenegro, 2008a. Inverse hydrochemical model of aqueous test. *Phys. Chem. Earth* 33, 1009–1018.

Zheng, L., J. Samper, L. Montenegro and J. C. Mayor, 2008b. Flow and reactive transport model of a ventilation experiment in Opallinus clay. *Phys. Chem. Earth* 33, S486–S498.

Zheng L., J. Samper, L. Montenegro and A.M. Fernández, 2010. A coupled model of heating and hydration laboratory experiment in unsaturated compacted FEBEX bentonite. *J. Hydrol.* 386, 80-94.

Zheng, L., J. Samper and L. Montenegro, 2011. A coupled THC model of the FEBEX in situ test with bentonite swelling and chemical and thermal osmosis. *J. Contam. Hydrol*. 126, 45–60.

Table 2. Qualitative comparison of the laboratory observations and model results for mineral dissolution/ precipitation. (LO = laboratory observations, MR = Model results, pre = precipitation, dis = dissolution, Port. = Portlandite, Calc. = Calcite, Bru. = Brucite, Qtz. = Quartz, Gyp. = Gypsum, Ettr. = Ettringite; Zeol.= zeolite; Hal. = Halite; K-feld. = K-feldspar; Chlo. = Chlorite; SP = Saponite; Vat. = vaterite; Tha. = Thaumasite; Ara. = Aragonite; Smect. Alt. = smectite alteration; Unalt. Bent.= Unaltered bentonite). The following symbols are used to indicate how well the model results reproduce the laboratory observations: ++ indicates good agreement, + means approximate agreement and – indicates no agreement. NC = not considered.

	Test HB1		Test HB2		Test HB3		Test HB4		Test HB5	Test HB6
	LO	**MR**	**LO**	**MR**	**LO**	**MR**	**LO**	**MR**	**LO**	**MR**
CONCRETE (hydration)	Port. dis	++	Port. dis	++	Port. dis	++			Port. dis	Port. dis
	Calc. pre	++	Calc. pre	++	Calc. pre	++	Calc. pre	++	Calc. pre	Calc. pre
	Bru. pre	++	Bru. pre	++	Bru. pre	++	Bru. pre	++	Bru. pre	Bru. pre
CONCRETE (30 mm)	Port. dis	++	Port. dis	++	Port. dis	++	Port. dis	++	Port. dis	Port. dis
		++	Calc. pre	++	Calc. pre	++	Calc. pre	++	Calc. pre	Calc. pre
	CSH pre	+	CSH pre	+	CSH pre	+	CSH pre	+	Some CSH pre	Some CSH pre
	Qtz. pre	-	Qtz. pre	-	Qtz. pre	-				
	MSH pre	++	MSH pre	++	MSH pre	++				
							Ettr. pre	-	No Ettr. pre	No Ettr. pre
					Gyp. pre	++				
					Tha. pre					
	Zeol. pre	NC	Hal. pre	NC	Vat. pre	NC				
			K-feld. pre		Ara. pre					
CONCRETE/ BENTONITE INTERFACE	Bru. pre	++	Bru. pre	++	Bru. pre	++	MSH pre	++	MSH pre	MSH pre
	Port. dis	-	Port. dis	-	Port. dis	-				
	Calc. pre	++	Calc. pre	++	Calc. pre	++	Calc. pre	++	Calc. pre	Calc. pre
	CSH pre	-	CSH pre	-	CSH pre	-	CSH(0.8) pre	-	No CSH pre	No CSH pre
			Ettr. pre	-	Ettr. pre	-	No Ettr. pre	++	No Ettr. pre	No Ettr. pre
			Gyp. pre	++	Gyp. pre	++				
					Qtz. dis	++				
	Not Smect. Alt.	NC	Smect. Alt.	NC	Smect. Alt.	NC				
					SP pre					
									Bru. pre	Bru. pre
BENTONITE							Calc. dis	++		
	Unalt. Bent.	+	Unalt. Bent.	+	Unalt. Bent.	+	Gyp. pre			
							Chlo. pre	++		